UCSF
UC San Francisco Previously Published Works

Title
Safety of retained microcatheters: an evaluation of radiofrequency heating in endovascular microcatheters with nitinol, tungsten, and polyetheretherketone braiding at 1.5 T and 3 T.

Permalink
https://escholarship.org/uc/item/9913g4tr

Journal
Journal of neurointerventional surgery, 6(4)

ISSN
1759-8478

Authors
Losey, Aaron D
Lillaney, Prasheel
Martin, Alastair J
et al.

Publication Date
2014-05-01

DOI
10.1136/neurintsurg-2013-010746

Peer reviewed

Safety of retained microcatheters: an evaluation of radiofrequency heating in endovascular microcatheters with nitinol, tungsten, and polyetheretherketone braiding at 1.5 T and 3 T

Aaron D. Losey, **Prasheel Lillaney**, **Alastair J. Martin**, **Van V. Halbach**, **Daniel L. Cooke**, **Christopher F. Dowd**, **Randall T. Higashida**, **David A. Saloner**, **Mark W. Wilson**, **Maythem Saeed**, and **Steven W. Hetts**
Department of Radiology and Biomedical Imaging, University of California, San Francisco, San Francisco, California, USA

Abstract

Background—The use of ethylene-vinyl alcohol copolymer for liquid embolization of cranial vascular lesions has resulted in microcatheter fragments entrapped in patients following endovascular procedures. Undergoing subsequent diagnostic MRI examinations poses a safety concern due to the possibility of radiofrequency heating of the metallic braid incorporated into the microcatheter. Heating of nitinol, tungsten, and polyetheretherketone (PEEK) braided microcatheters was assessed and compared using a phantom model.

Methods—Microcatheters coupled with fluoroptic temperature probes were embedded in a polyacrylamide gel within a head and torso phantom. Experiments were performed at 1.5 T and 3 T, analyzing the effects of different catheter immersion lengths, specific absorption rate (SAR) levels, short clinical scans, long clinical scans, and microcatheter fragment lengths.

Results—The maximal increase in temperature for the nitinol braided microcatheter during a 15 min scan was 3.06°C using the T1 fast spin echo sequence at 1.5 T and 0.45°C using the balanced steady state free precession sequence at 3 T. The same scans for fragment lengths of 9, 18, 36, and 72 cm produced maximal temperature rises of 0.68, 0.80, 1.70, and 1.07°C at 1.5 T, respectively. The temperature changes at 3 T for these fragment lengths were 0.66, 0.83, 1.07, and 0.72°C, respectively. The tungsten and PEEK braided microcatheters did not demonstrate heating.

Conclusions—Substantial heating of nitinol braided microcatheters occurred and was a function of SAR level and geometric considerations. SAR and time limitations on MR scanning are proposed for patients with this microcatheter entrapped in their vasculature. In contrast, tungsten and PEEK braided microcatheters showed potential safe use in MRI.

Correspondence to: Mr A D Losey, Department of Radiology and Biomedical Imaging, University of California, San Francisco, San Francisco, 185 Berry Street, Suite 350, San Francisco, CA 94107, USA; Aaron.Losey@ucsf.edu.

INTRODUCTION

Endovascular treatment of cranial and spinal lesions, such as arteriovenous malformations and arteriovenous fistulas, using liquid embolic material is becoming more common.[1] Ethylene-vinyl alcohol copolymer (EVOH; Onyx, Covidien, Irvine, California, USA) is a newer liquid embolic material supplied in dimethyl sulfoxide, used to treat these lesions via microcatheter delivery. Along with its non-adhesive nature, the potential benefit of EVOH over n-butyl 2-cyanoacrylate is longer polymerization time which allows for slower filling and better penetration of vascular lesions.[2] However, despite these benefits, the use of EVOH has resulted in microcatheter fragments of varying lengths, occasionally left in place in patients following embolization procedures.[3–12] Some of the entrapped microcatheters were removed,[13–16] yet many remain permanently. For example, Weber et al reported a retained catheter rate of 4% for arteriovenous malformations while Natarajan et al experienced a rate of 8% in adults treated for dural arteriovenous fistulas.[711] Ashour et al[4] reported two cases (1.9%) of retained microcatheters in children embolized with EVOH. The overall incidence of retained microcatheters in unknown, yet the increase in reports resulted in the US Food and Drug Administration (FDA) releasing a Safety Communication to summarize the problem and inform physicians and patients about the risk of catheter entrapment.[17] Additionally, this problem has come to the attention of manufacturers, and a new detachable microcatheter was designed to overcome the complications associated with device retention.[18] Nevertheless, there is a patient population facing the long term consequences of a retained microcatheter or microcatheter fragment.

While short term complications of retained microcatheters have been well studied, little information is available on long term effects.[6] These microcatheters often contain metallic braiding extending along the majority of the shaft (figure 1A, B). This component provides desirable intraprocedural properties such as adequate torque response at the microcatheter tip when proximal manipulation is applied. However, for patients with retained microcatheters, subsequent diagnostic MRI examinations pose a safety concern due to the possibility of radiofrequency (RF) heating of the microcatheter metallic braid.[19] This phenomenon has been studied and documented for endovascular guidewires and larger catheters[20–22] but not for smaller microcatheters typically used to deliver liquid embolics. Thus there is a need to determine the criteria for safe MR scanning in the presence of retained microcatheters.

The purpose of this study was to explore the factors that can potentially affect the magnitude of catheter heating, such as specific absorption rate (SAR) level, scanning sequence, microcatheter length, and braided material at different MR magnetic field strengths. Heating of nitinol, tungsten, and polyetheretherketone (PEEK) braided microcatheters was assessed in an in vitro phantom model simulating a patient undergoing clinical scans with a range of SAR levels.

MATERIALS AND METHODS

Experiments

We conducted a phantom study to detect change in temperature surrounding endovascular microcatheters during scans on two clinical MR systems: 1.5 T (Philips Achieva, Cleveland, Ohio, USA) and 3 T (GE Discovery 750w, Milwaukee, Wisconsin, USA). The 1.5 T system has a 60 cm diameter bore and the 3 T system features a 70 cm diameter bore. Body coil RF transmission was used for all studies.

A phantom (figure 1C) conforming to the dimensions listed in ASTM F2182-02 for the torso was created from clear acrylic sheets. This phantom features two distinct and continuous

sections corresponding to the head and body portions of the phantom. In initial studies, the head portion of the phantom contained a polyacrylamide gel (6.5% acrylamide, 0.3% bisacrylamide, 0.05% TEMED, and 0.08% ammonium persulfate) in deionized water doped with 0.35% sodium chloride. In subsequent studies, both the head portion and body portion contained polyacrylamide gel. For each scan the phantom was centered mediolaterally and inserted such that the center of the head portion was at isocenter.

All microcatheters embedded and tested in the phantom were prescreened to assure that they experienced no magnetic deflection at the bore opening of the MR systems. Heating immediately adjacent to the microcatheters was assessed with fluoroptic temperature probes (FOT Lab Kit and STF probes; LumaSense, Santa Clara, California, USA) that were attached in a side by side fashion. Temperature probes were secured to the catheters with silk suture to assure good contact over the last 2 cm of the temperature probe. Up to six independent sensors could be sampled at 1 Hz and all sensors were embedded in gel to minimize thermal convection effects. One channel was reserved for a background gel sensor, positioned well away from the conductive structures, and the remaining sensors were positioned at varying points on the microcatheter.

Heating in three microcatheters containing unique braiding was assessed with a series of five experiments conducted with different MR system strengths, SAR levels, scanning sequences, microcatheter configurations, and lengths.

Experiment 1: immersion length—The first set of experiments was performed to investigate which immersion length provided the greatest heating. A 1.9 F nitinol braided microcatheter (Covidien Echelon-14, Irvine, California, USA), 2.8 F tungsten braided microcatheter (Terumo Progreat, Somerset, New Jersey, USA), and custom 2.7 F PEEK braided microcatheter (Penumbra, Alameda, California, USA) were serially embedded in a laterally offset configuration, 17 cm from the midline in the body portion and 6 cm from the midline in the head portion on the phantom. The offset position was used to simulate the worst case scenario in a patient. Each catheter extended 25 cm into the head portion, which was made of polyacrylamide gel. The body portion featured an aqueous solution of 0.35% sodium chloride to permit conformational changes to the catheters. Temperature probes were placed at the catheter's distal tip and 5, 10, and 20 cm proximal to the tip. A 5 F stainless steel braided catheter (Cook Beacon Tip Torcon Advantage VERT, Bloomington, Indiana, USA) was used as a positive control with a temperature probe placed at the tip of the catheter, based on prior experiments demonstrating this catheter's propensity to heat on two separate 1.5 T systems.[20] The catheters were immersed at 98 cm and imaged for 2 min using a fast spin echo (FSE) sequence at 1.5 T with a SAR of 4 W/kg followed by 8 min without scanning. The immersed length was shortened by 5 cm and this cycle was repeated until the immersed length was 63 cm. MR scanning was repeated at 3 T with a SAR of 3.5 W/kg.

Experiment 2: SAR scaling—Quantitative analysis was subsequently performed on the nitinol and tungsten braided microcatheters. Each catheter was serially embedded in the offset configuration using a solid gel throughout the phantom that showed the worst heating in previous experiments, which was 93 cm immersed. Temperature probes were placed at the catheter distal tip and 20, 40 (shoulder), 65, and 90 cm proximal to the tip. The impact of different SAR levels was measured by scaling SAR between 0.25 and 4.0 W/kg at 1.5 T and between 0.35 and 3.5 W/kg at 3 T while holding the other parameters constant. The catheters were exposed to 2 min of scanning at each SAR level followed by 8 min without scanning.

Experiment 3: short clinical scans—The nitinol and tungsten braided microcatheters were serially embedded along with the temperature probes in the same configuration as experiment 2. In order to assess the effect of different clinical sequences, the following imaging sequences were performed: diffusion weighted imaging (DWI), balanced steady state free precession (b-SSFP), spoiled gradient echo (3D-SPGR), T2 fluid attenuated inversion recovery (T2 FLAIR), T1 FSE, and T2 FSE for 2 min of scanning followed by 8 min without scanning at 1.5 T and 3 T (table 1).

Experiment 4: long clinical scans—The nitinol and tungsten braided microcatheters and temperature probes were serially embedded in the same configuration as in experiment 2. In order to assess the maximum change in temperature over a long period of time, the scans that produced the worst heating at each magnetic field strength during the short clinical scans were repeated for a full 15 min acquisition: T1 FSE at 1.5 T and b-SSFP at 3 T, followed by 10 min without scanning.

Experiment 5: catheter fragments—A more detailed analysis was subsequently performed on nitinol braided microcatheter fragments due to their propensity for heating and the common clinical use of nitinol braided catheters in delivery of liquid embolic material. Fragments 9, 18, 36, and 72 cm in length were serially embedded in an anatomical configuration, 9 cm from the midline in the body portion and 2.5 cm from the midline in the head portion on the phantom. Each catheter fragment extended 13 cm into the head portion. The anatomical position was used to simulate a clinically relevant position in a patient. A solid polyacrylamide gel covered the entire length of each fragment. Temperature probes were placed at the catheter's distal tip and proximal end with additional probes placed along the length of the catheter depending on the fragment size. An additional sensor was also used to measure the background gel temperature. As in experiment 3, the following clinical scans were repeated: DWI, b-SSFP, 3D-SPGR, T2 FLAIR, T1 FSE, and T2 FSE for 2 min of scanning followed by 8 min without scanning. The scans that produced the worst heating were repeated for a full 15 min acquisition: T1 FSE at 1.5 T and b-SSFP at 3 T, followed by 10 min without scanning.

Statistical analysis

Heating data were analyzed using MATLAB (The Mathworks Inc, Natick, Massachusetts, USA), and initial rate of temperature change and absolute temperature change were calculated from each experiment. The former was measured by fitting the temperature during the first 20 s of scanning to a linear function and extracting maximum slope. The latter was obtained by subtracting the minimum temperature from the maximum temperature during the scan.

RESULTS

Experiment 1: immersion length

Maximal heating for the nitinol braided microcatheter occurred at 20 cm proximal to the tip at an immersed length of 93 cm for 1.5 T and 3 T. As the catheter was embedded 25 cm into the head, this corresponds to the neck region of the phantom before the catheter turned toward the shoulder. The maximal initial rate of heating was 4.00 °C/min at 1.5 T and 1.00 °C/min at 3 T. The maximal temperature rise during a 2 min scan was 2.32°C at 1.5 T and 0.58°C at 3 T. At all points along the microcatheter embedded in the head region there were maximum temperature rises greater than 1.0°C at 1.5 T. At 3 T, the device tip, 5 and 10 cm from the tip, demonstrated a temperature response indistinguishable from the background sensor; only 20 cm proximal to the tip showed measurable heating. Maximum temperature rises greater than 0.50°C were consistent at 20 cm proximal to the tip at 3 T. The tungsten

and PEEK braided microcatheters did not show heating and demonstrated a temperature response consistent with the background sensor for this and the following experiments. The maximal temperature rise during a 2 min scan was 0.31 and 0.30 °C for the negative control background sensor at 1.5 T and 3 T, respectively. The maximal temperature rise during a 2 min scan was 3.65 and 0.66 °C for the positive control stainless steel catheter at 1.5 T and 3 T, respectively.

Experiment 2: SAR scaling

Scaling SAR level and controlling other parameters tested the assumption that SAR correlates linearly with heat deposition. Our results for the nitinol braided microcatheter at 1.5 T showed the initial heating rate of the temperature sensors for different SAR levels were consistent with previous experiments.[20] The sensors exhibiting the greatest heating (tip, 20, 40 cm) displayed a linear correlation between SAR and heating (R^2=0.83, R^2=0.91, R^2=0.80, respectively). For SAR levels at 3 T, the actual heating rate was obscured by the noise of the measurement. Likewise, the tungsten braided microcatheter that demonstrated temperature response equivalent to the background sensor did not show a relationship with SAR due to the lack of heating.

Experiment 3: short clinical scans

The microcatheter heating differences in the nitinol braided microcatheter among common clinical scans were explored and are presented in table 1.

Experiment 4: long clinical scans

T1 FSE at 1.5 T and b-SSFP at 3 T resulted in the most heating of the nitinol braided microcatheter, as shown in figure 2.

Experiment 5: catheter fragments

Heating levels of different nitinol braided catheter fragment lengths were tested in an anatomical conformation to more closely reflect clinical scenarios in which catheter fragments break or are retained and cut at the femoral artery. Both the short and long clinical scans from experiments 3 and 4 were performed. The results of the short clinical scans reflected the results of experiment 3, with all 2 min scans with a predicted average SAR of >1.5 W/kg demonstrating heating. At 3 T, sequences with a predicted average SAR of >2.40 W/kg demonstrated heating. The results of the long clinical scans showed variation in heating depending on catheter length, as shown in table 2.

DISCUSSION

This study provides information on the magnitude of focal heating induced in a head and body phantom adjacent to an endovascular microcatheter or fragment in 'worst case' scenarios (experiment Nos 1–4) and clinical simulated scenarios (experiment No 5) of a patient undergoing MRI scans at a range of SAR levels. Nitinol braided catheters heated significantly more than tungsten and PEEK braided devices. In the case of the nitinol braided microcatheter, the higher reported potential SAR level resulted in more heating above a certain threshold. Additionally, more heating occurred at 1.5 T compared with 3 T at similar reported SAR levels. Shorter microcatheter fragments produced less heating. The one exception to this trend was the increase in heating seen in the 36 cm fragment relative to the other fragments.

Our results suggest that this specific nitinol braided catheter heated more than the microcatheters with tungsten or PEEK braiding tested. This is not a commentary on these materials under all conditions, but rather specific to these microcatheters. The differences in

heating are likely based on microcatheter design: including French size, length, pitch, and thickness of the braiding. The scope of this study was not to account for every type of microcatheter, but on a subset. This study does provide, however, quantitative data on the magnitude of heating that could be induced in a nitinol braided catheter commonly used to delivery EVOH. Our results are consistent with a previous study using the same methodology that showed initial heating rates of 0.33–1.90°C/min.[20] Given that FDA MRI safety guidelines specify <1°C heating in the head and <2°C heating in the body, methods for safely tailoring MR imaging to the diagnostic needs of a patient with a retained catheter fragment should be explored. It is encouraging, however, that no dramatic rapid catheter heating was observed in our experiments.

With regard to a higher reported potential SAR level resulting in more heating, this relationship is often assumed but has rarely been documented.[20] Some have argued that the use of the RF electromagnetic field, $B1_{rms}$, is more appropriate to evaluate implant heating in phantoms,[23] however, there is no evidence that use of $B1_{rms}$ is better than the MR system reported SAR value.[24] The higher heating at 1.5 T compared with 3 T is consistent with a study done on cardiac pacemakers.[25] There are likely to be multiple contributing factors that are difficult to quantify yet the leading hypotheses explaining our results are as follows. First, this likely is a result of more restrictive SAR models that are employed at higher field strengths. The SAR listed with an MR scan is a prediction of energy deposition and is subject to a number of assumptions. Second, the 1.5 T scanning system was a short bore and the 3 T system was a wide bore with different bore diameters. It is possible that the greater distance of the phantom from the electric fields of the body coil in the 3 T system resulted in less heating of the microcatheter. Both of these hypotheses highlight the importance of fully characterizing the MR system and microcatheters that are to be studied before proposing conditions under which human studies may be performed with minimal risk of thermal injury.

The length of each microcatheter fragment was based on clinical relevance and the potential for resonant heating. Resonant heating is maximized when the conductor length is an integer multiple of half the wavelength of RF energy.[26] The wavelength in tissue is approximately 36 cm at 1.5 T and 18 cm at 3 T, making the approximate resonance lengths 18 cm and 9 cm long, respectively.[27] We tested catheter fragments that were half wavelength, wavelength, and an integer multiple of two wavelengths in each MR system, which did not reveal strongly resonant effects. It is likely that considering the length of a microcatheter implant alone is too simplistic as other factors influence MRI related heating.[20,24] The plastic into which the braiding is embedded and the actual length of the braiding instead of the microcatheter fragment length likely alter the heating behavior. Intentionally designing a predictable break point or detachment point into microcatheters (whether they are intended to be implanted or not) would simplify the assessment of catheter fragment length safety.

The methodologies used in this study are comparable with previous studies that assessed MRI related heating of larger catheters, guidewires, and other implantable devices,[20,28–30] but are not without limitations. Fluoroptic thermometry is designed for the MR system but the temperature sensor itself is small, therefore only measuring temperature over a finite volume immediately adjacent to the microcatheters. The polyacrylamide gel model simulates heating of static tissue (without blood flow). It is expected that blood flow would decrease temperature elevations. No induction loops (the microcatheter looping back on itself, such as in a very tortuous vessel) were tested in the current study. It is possible that a loop would create a structure more efficient at picking up RF energy, therefore resulting in larger temperature elevations. Future research should focus on a broader scope of microcatheters with more geometric configurations to evaluate a range of torturous geometries relevant to the cervicocerebral vasculature. Additionally, to fully assess the

effect of blood flow, in vivo experiments measuring temperature change in the presence and absence of flow should be considered.

CONCLUSION

RF induced heating of nitinol braided microcatheters occurs during MR imaging and is a function of SAR level and geometric considerations. SAR (<1 W/kg at 1.5 T and <2 W/kg at 3 T) and time limitations are proposed for patients with this microcatheter retained in their vasculature. In contrast, selected tungsten and PEEK braided microcatheters showed potential safe use during MRI without SAR restrictions, thus suggesting alternate materials with which to braid neurovascular microcatheters.

Acknowledgments

References

1. Radvany MG, Gregg L. Endovascular treatment of cranial arteriovenous malformations and dural arteriovenous fistulas. Neurosurg Clin N Am. 2012; 23:123–31. [PubMed: 22107863]

2. Jahan R, Murayama Y, Gobin YP, et al. Embolization of arteriovenous malformations with Onyx: clinicopathological experience in 23 patients. Neurosurgery. 2001; 48:984–95. [PubMed: 11334300]

3. Panagiotopoulos V, Gizewski E, Asgari S, et al. Embolization of intracranial arteriovenous malformations with ethylene-vinyl alcohol copolymer (Onyx). AJNR Am J Neuroradiol. 2009; 30:99–106. [PubMed: 18842759]

4. Ashour R, Aziz-Sultan MA, Soltanolkotabi M, et al. Safety and efficacy of Onyx embolization for pediatric cranial and spinal vascular lesions and tumors. Neurosurgery. 2012; 71:773–84. [PubMed: 22989958]

5. Carlson AP, Taylor CL, Yonas H. Treatment of dural arteriovenous fistula using ethylene vinyl alcohol (Onyx) arterial embolization as the primary modality: short-term results. J Neurosurg. 2007; 107:1120–5. [PubMed: 18077948]

6. Lee JI, Choi CH, Ko JK, et al. Retained microcatheter after Onyx embolization of intracranial arteriovenous malformation. J Korean Neurosurg Soc. 2012; 51:374–6. [PubMed: 22949969]

7. Natarajan SK, Ghodke B, Kim LJ, et al. Multimodality treatment of intracranial dural arteriovenous fistulas in the Onyx era: a single center experience. World Neurosurg. 2010; 73:365–79. [PubMed: 20849795]

8. Puri AS, Rahbar R, Dearden J, et al. Stretched and sheared microcatheter retained after Onyx embolization of infantile myofibromatosis. Interv Neuroradiol. 2011; 17:261–6. [PubMed: 21696669]

9. Renieri L, Consoli A, Scarpini G, et al. Double arterial catheterization technique for embolization of brain arteriovenous malformations with Onyx. Neurosurgery. 2013; 72:92–8. [PubMed: 23096412]

10. Weber W, Kis B, Siekmann R, et al. Preoperative embolization of intracranial arteriovenous malformations with Onyx. Neurosurgery. 2007; 61:244–52. [PubMed: 17762736]

11. Weber W, Kis B, Siekmann R, et al. Endovascular treatment of intracranial arteriovenous malformations with Onyx: technical aspects. AJNR Am J Neuroradiol. 2007; 28:371–7. [PubMed: 17297015]

12. Cognard C, Januel AC, Silva NA Jr, et al. Endovascular treatment of intracranial dural arteriovenous fistulas with cortical venous drainage: new management using Onyx. AJNR Am J Neuroradiol. 2008; 29:235–41. [PubMed: 17989374]

13. Bingol H, Sirin G, Akay HT, et al. Management of a retained catheter in an arteriovenous malformation. Case report J Neurosurg. 2007; 106:481–3.

14. Kelly ME, Turner Rt, Gonugunta V, et al. Monorail snare technique for the retrieval of an adherent microcatheter from an Onyx cast: technical case report. Neurosurgery. 2008; 63:ONSE89. [PubMed: 18728613]

15. Santillan A, Zink W, Knopman J, et al. Balloon-assisted technique for trapped microcatheter retrieval following Onyx embolization. A case report Interv Neuroradiol. 2009; 15:453–5.

16. Walcott BP, Gerrard JL, Nogueira RG, et al. Microsurgical retrieval of an endovascular microcatheter trapped during Onyx embolization of a cerebral arteriovenous malformation. J Neurointerv Surg. 2011; 3:77–9. [PubMed: 21990795]

17. U.S. Food and Drug Administration. [accessed 14 Dec 2012] Safety communication: catheter entrapment with the ev3 Onyx liquid embolic system. Nov 20. 2012 http://www.fda.gov/MedicalDevices/Safety/AlertsandNotices/ucm310121.htm

18. Maimon S, Strauss I, Frolov V, et al. Brain arteriovenous malformation treatment using a combination of Onyx and a new detachable tip microcatheter, SONIC: short-term results. AJNR Am J Neuroradiol. 2010; 31:947–54. [PubMed: 20190210]

19. Shellock FG. Radiofrequency energy-induced heating during MR procedures: a review. J Magn Reson Imaging. 2000; 12:30–6. [PubMed: 10931562]

20. Martin AJ, Baek B, Acevedo-Bolton G, et al. MR imaging during endovascular procedures: an evaluation of the potential for catheter heating. Magn Reson Med. 2009; 61:45–53. [PubMed: 19097197]

21. Konings MK, Bartels LW, Smits HF, et al. Heating around intravascular guidewires by resonating RF waves. J Magn Reson Imaging. 2000; 12:79–85. [PubMed: 10931567]

22. Nitz WR, Oppelt A, Renz W, et al. On the heating of linear conductive structures as guide wires and catheters in interventional MRI. J Magn Reson Imaging. 2001; 13:105–14. [PubMed: 11169811]

23. Kainz W. MR heating tests of MR critical implants. J Magn Reson Imaging. 2007; 26:450–1. [PubMed: 17729357]

24. Shellock FG. Comments on MR heating tests of critical implants. J Magn Reson Imaging. 2007; 26:1182–5. [PubMed: 17969159]

25. Shellock FG, Valencerina S, Fischer L. MRI-related heating of pacemaker at 1. 5- and 3-Tesla: evaluation with and without pulse generator attached to leads. Circulation. 2005; 112(Suppl II): 561.

26. Ladd ME, Quick HH. Reduction of resonant RF heating in intravascular catheters using coaxial chokes. Magn Reson Med. 2000; 43:615–19. [PubMed: 10748440]

27. Atalar E. Radiofrequency safety for interventional MRI procedures. Acad Radiol. 2005; 12:1149–57. [PubMed: 16112515]

28. Finelli DA, Rezai AR, Ruggieri PM, et al. MR imaging-related heating of deep brain stimulation electrodes: in vitro study. AJNR Am J Neuroradiol. 2002; 23:1795–802. [PubMed: 12427641]

29. Rezai AR, Finelli D, Nyenhuis JA, et al. Neurostimulation systems for deep brain stimulation: in vitro evaluation of magnetic resonance imaging-related heating at 1. 5 tesla. J Magn Reson Imaging. 2002; 15:241–50. [PubMed: 11891968]

30. Shellock FG, Fischer L, Fieno DS. Cardiac pacemakers and implantable cardioverter defibrillators: in vitro magnetic resonance imaging evaluation at 1. 5-tesla. J Cardiovasc Magn Reson. 2007; 9:21–31. [PubMed: 17178677]
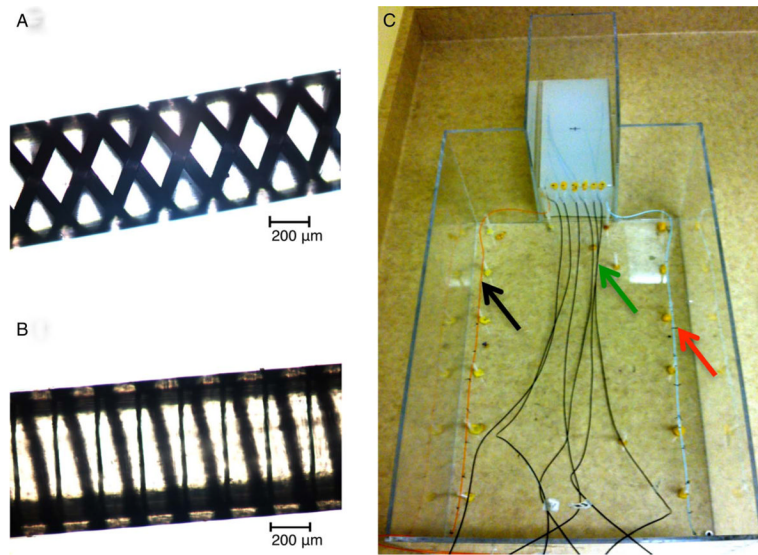
Figure 1.
Metallic braiding of microcatheters and phantom. (A, B) Microphotographs of (A) a nitinol braided microcatheter and (B) a tungsten braided microcatheter. (C) The phantom with head portion gelled containing a polyetheretherketone (PEEK) braided microcatheter (black arrow) and a stainless steel braided catheter (red arrow) with adjacent temperature sensors (green arrow).
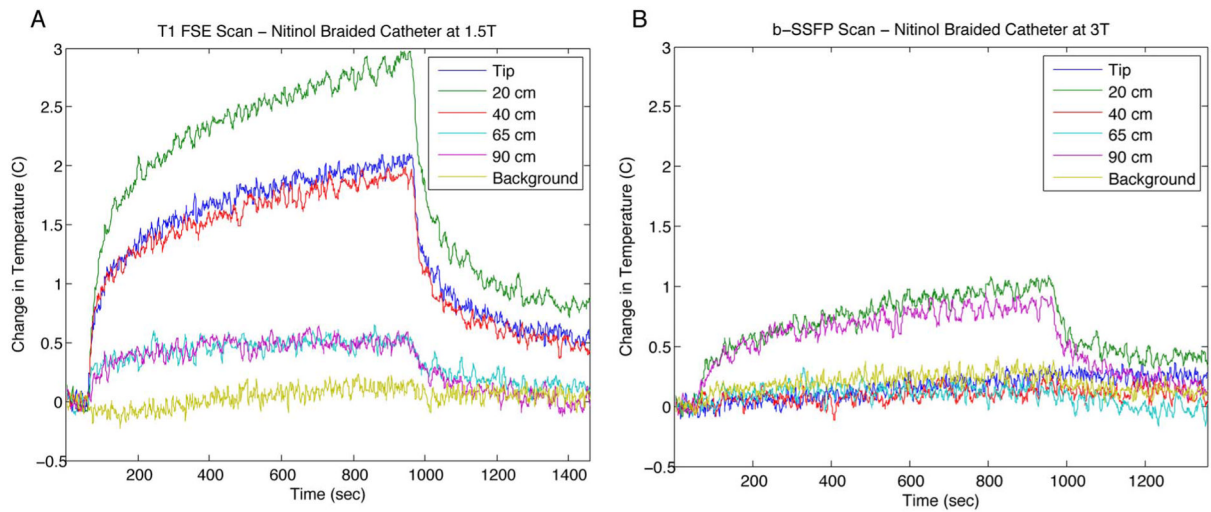
Figure 2.
Temperature change at different points along the nitinol braided catheter over 15 min. (A) T1 fast spin echo (FSE) scan at 1.5 T. (B) Balanced steady state free precession (b-SSFP) scan at 3 T.

Table 1

MR imaging sequences and maximum change in temperature of the nitinol braided microcatheter at 1.5 T and 3 T

	DWI	b-SSFP	SPGR	T2 FLAIR	T1 FSE	T2 FSE
Imaging parameters at 1.5 T						
TR (ms)	3692.0	6.4	20.0	10200.0	427.0	5038.0
TE (ms)	81	3.2	3.8	140	12	113
Matrix (pixels)	128×77	256×227	240×190	252×141	256×137	400×205
Average SAR	0.4	2.0	0.6	1.6	4.0	3.0
Heating at 1.5 T						
Change in temperature (°C)	–	0.52	–	0.73	0.84	0.72
Distance from the tip (cm)	–	20	–	20	20	20
Imaging parameters at 3 T						
TR (ms)	8000.0	4.4	7.5	9500.0	700.0	5000.0
TE (ms)	Min–Full	Min	Min–Full	120	Min–Full	102
Matrix (pixels)	128×128	256×160	256×256	352×128	512×320	512×256
Average SAR	0.58	2.90	0.59	1.24	2.43	1.16
Heating at 3 T						
Change in temperature (°C)	–	0.45	–	–	0.44	–
Distance from the tip (cm)	–	20	–	–	20	–

–, temperature response equivalent to the background sensor; b-SSFP, balanced steady state free precession; DWI, diffusion weighted imaging; FLAIR, fluid attenuated inversion recovery; FSE, fast spin echo; SAR, specific absorption rate; SPGR, spoiled gradient echo; TE, echo time; TR, repetition time.

Table 2

Maximum change in temperature of nitinol braided catheter fragments during T1 fast spin echo at 1.5 T and balanced steady state free precession at 3 T

	Fragment length (cm)			
	9	**18**	**36**	**72**
Maximum change in temperature (°C)	0.68	0.80	1.70	1.07
Distance from the tip (cm)	0	0	27	18
Maximum change in background temperature (°C)	0.48	0.48	0.42	0.42
Maximum change in temperature (°C)	0.66	0.83	1.07	0.72
Distance from the tip (cm)	9	18	18	18
Maximum change in background temperature (°C)	0.32	0.32	0.36	0.43